9-1 (Invited)

The Process Modeling Hierarchy: Connecting Atomistic Calculations to Nanoscale Behavior

Scott T. Dunham
University of Washington, Department of Electrical Engineering
Box 352500, Seattle, WA, 98105, USA
Email: dunham@ee.washington.edu

***Abstract* — In this work, we review efforts to make effective use of atomistic calculations for the advancement of VLSI process simulation.**

I. INTRODUCTION

Accurately predicting nanoscale device structures resulting from advanced integrated circuit fabrication processes is a very challenging problem due to the large number of strongly interacting reactions, the dominance of non-equilibrium behavior, and the fine tolerances required. Great advances have been made in understanding ion implantation, defect-mediated dopant diffusion, extended defect kinetics and film growth along with their interactions, but many mysteries still remain. Atomistic techniques provide a range of powerful tools including *ab-initio* calculations based on density functional theory (DFT), empirical-potential molecular dynamics (MD), and kinetic Monte Carlo (MC). These tools have the potential to significantly advance the predictive capability of process simulators. However, substantial challenges must be overcome to make effective use of such calculations due to the wide gap which is present in the spatial and temporal scales.

Figure 1: Hierarchy of process modeling approaches. Results from more fundamental calculations are used in higher level modeling.

II. APPLICATION OF DFT CALCULATIONS

We begin by discussing direct application of *ab-initio* calculations to guide continuum modeling. The accuracy of these calculations is still generally insufficient for their direct use in quantitative prediction of device structures. Instead, their main role lies in identifying the most likely reaction paths and dominant or rate-limiting process among the complex array of possibilities.

An important example of direct application of DFT calculations to continuum simulations is boron interstitial cluster (BIC) formation. It is logical to expect boron to aggregate in association with interstitials due to size differences, but there exists an immense range of possible cluster structures, compositions and formation paths (and associated large number of potential model parameters). DFT calculations of cluster formation energies [1, 2] identify B_3I clusters as the most prominent cluster limiting B activation.

In order to identify the most likely paths for cluster formation, it is necessary to investigate the barriers associated with the cluster formation process. Identification and quantification of transition barriers for cluster formation using the dimer [3] and nudged elastic band [4] methods leads to several notable results [5] (Fig. 2): formation of the key intermediate species B_3I_2 is diffusion limited for both $B_2I + BI$ and $B_3I + I$; B_3I_2 has multiple structures with nearly equal energy, separated by a substantial (~1.5eV) barrier (this barrier limits the rate of transformation from $B_2I + BI$ to $B_3I + I$); and formation/dissociation of B_3I to $B_2 + BI$ is energetically unfavorable.

Based on these DFT results, we have developed a continuum model for B clustering kinetics. The dominant cluster for all but very short times or very high doping levels (for which small or large clusters become significant) is B_3I. For midgap Fermi levels, B_3I is negatively charged, but B clustering occurs in strongly p-type material for which the neutral cluster is favored [2]. The kinetics of B_3I are limited by the formation and dissociation of B_3I_2:

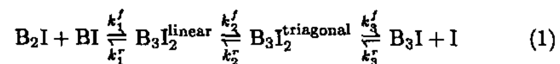

$$B_2I + BI \underset{k_1^r}{\overset{k_1^f}{\rightleftharpoons}} B_3I_2^{\text{linear}} \underset{k_2^r}{\overset{k_2^f}{\rightleftharpoons}} B_3I_2^{\text{triagonal}} \underset{k_3^r}{\overset{k_3^f}{\rightleftharpoons}} B_3I + I \qquad (1)$$

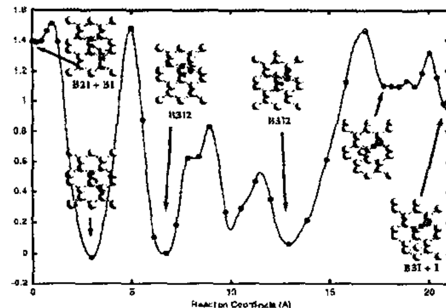

Figure 2: Minimum energy path within a neutral system for the capture of a BI pair by an B_2I cluster and subsequent ejection of I forming B_3I (from Uberuaga *et al.* [5]).

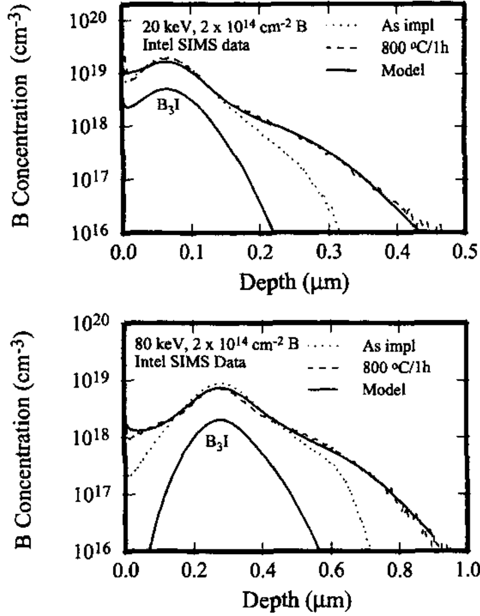

Figure 3: Comparison of simulation to experimental data for $2 \times 10^{14}\,\mathrm{cm}^{-2}$ 20 keV and 80 keV boron implants after a 1 h anneal at 800°C. SIMS data from Intel.

For all but extremely short times, the concentration of B_2I approaches local equilibrium with the B and I concentrations [6]. Based on DFT calculations [5], the first and last reactions (k_{1f} and k_{3r}) are diffusion limited, while the middle reaction has a substantial barrier [5]. We can thus write the net formation rate of B_3I as $R_{\mathrm{B_3I}} = k_1^f \gamma \left[C_{\mathrm{B_2I}} C_{\mathrm{BI}} - K C_{\mathrm{B_3I}} C_{\mathrm{I}}\right]$, where γ is the probability of $B_3I_2^{linear}$ dissociating to $B_3I + I$ rather than $B_2I + BI$. The system is equivalent to the model we previously reported [6], except that the barrier for B_3I_2 transformation reduces the forward rate. Figure 3 show comparisons of the resulting model to experimental data. The simulations include a five-stream model for dopant diffusion and an analytic moment-based model for {311} evolution [7].

Fluorine has been shown to have beneficial properties on both boron TED reduction [8-11] as well as boron activation [8, 9]. However, to utilize these benefits effectively, a fundamental understanding of F behavior is necessary, particularly since implanted F shows anomalous diffusion behavior [12]: instead of a broadening, annealed profiles first remain immobile and then sharpen and shift toward the surface (Fig. 4).

Based on DFT calculations [13], a single F atom prefers to reside in a bond centered interstitial site. This site is preferred by 0.18 eV over the tetrahedral interstitial configuration and by 1.00 eV over the lowest substitutional site. Interstitial F is highly mobile ($E_m = 0.73$ eV). No F/I clusters with significant binding energies have been identified. However, we found F_nV_m structures to have high binding energies (see Table 1), with F potentially saturating all the dangling bonds associated with small V clusters (e.g., 4 F for V, 6 F for V_2) [13]. For two or more F atoms, F_nV_m clusters are energetically favorable even when the formation energy of V are considered. The saturated F_6V_2 structure is even stable in the presence of interstitials (binding energy exceeds Frenkel pair formation energy). Because of this strong binding, F can be expected to reside in F_nV_m structures during initial stages of implant anneals due to the presence of excess vacancies.

Structure	E_b last F [eV]	E_b^{tot} [eV]	E_f [eV]
FV	−2.38	−2.38	+1.00
F_2V	−2.25	−4.63	−1.25
F_3V	−1.95	−6.58	−3.20
F_4V	−0.54	−7.12	−3.74
V_2	—	−1.45	+5.31
FV_2	−2.75	−4.20	+2.56
F_2V_2	−2.87	−7.07	−0.31
F_3V_2	−1.97	−9.04	−2.28
F_4V_2	−2.43	−11.47	−4.71
F_5V_2	−1.82	−13.29	−6.53
F_6V_2	−1.80	−15.09	−8.33

Table 1: Binding energies of F_nV_m configurations. The decreasing binding energy of the F_nV structures is attributed to the increasing crowding of the F atoms. The total binding energies (third column) are calculated with respect to interstitial fluorine (F_i) and single vacancies (V). The binding energies in the second column are the energy change in adding an additional F to the structure. The fourth column lists the total formation energy, which includes the formation energy of the necessary vacancies.

When F_i diffusion along with fluorine decoration of V and V_2 is included in a continuum model along with standard point defect diffusion/clustering models, the resulting simulation profiles correctly predict the apparent uphill diffusion observed experimentally during annealing of implanted F (Fig. 4). This behavior is due to the F_nV_m dissolving in the deeper I-rich regions, but remaining in the shallow V-rich regions.

Initial DFT results indicate no significant B/F clusters [13]. However, they do suggest a possible source for the desirable effect of F on B shallow junction formation. Due to the strong affinity of F for V, in amorphized samples we expect incorporation of F_nV_m clusters during regrowth. The consequences for boron diffusion in such an environment would be TED reduction and enhanced activation for pre-amorphized samples due to grown-in V, consistent with experimental results [8-11].

III. KINETIC LATTICE MONTE CARLO

Although atomistic calculations can in many cases be used effectively in continuum simulations, many other processes occurring on the atomic scale are not accurately replicated in continuum models. At the same time,

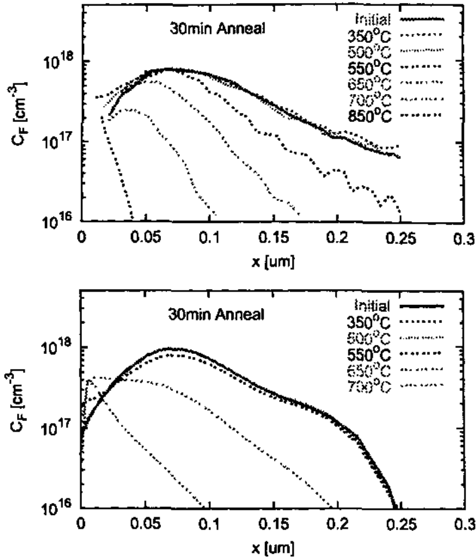

Figure 4: Comparison of simulation (bottom) with experimental data [12] (top) for 10^{13}cm^{-2} 30 keV F^+ implant annealed for 30 min at various temperatures. The simulation includes F_nV, F_nV_2, and FI clusters in addition to an extended defect model [7]. The initial defect/fluorine profiles were obtained with UT-Marlowe.

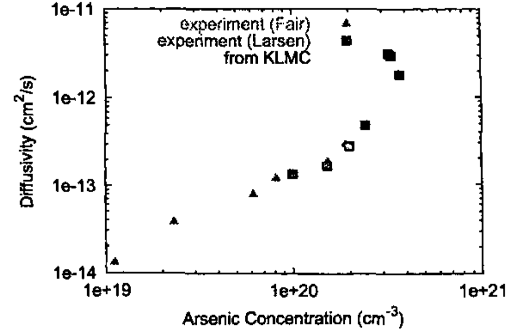

Figure 5: Comparison of LMC predictions to experimental measurement of arsenic diffusivity at 1050°C versus doping level [19, 20]. The diffusivity for moderate doping levels is fit assuming diffusion via negatively-charged vacancies and then extrapolated to higher doping levels using the LMC simulation results. Note a sharp increase in arsenic diffusivity for donor concentrations exceeding 2×10^{20} cm^{-3}.

MD simulations are generally limited to times on the order of μs. To bridge this gap, we have developed a kinetic lattice Monte-Carlo (KLMC) approach [14-16]. The strength of KLMC is that at the fundamental level, most processes involve jumps between locally stable configurations. Thus, the underlying time scale is the hop frequency (~ns) rather than the vibration frequency (<ps). In addition, by considering only the behavior of mobile species (e.g., point defects), the number of active sites is many orders of magnitude smaller than the lattice density. Therefore, it is possible to maintain the underlying atomic structure and mechanisms and yet also consider system sizes and process times appropriate to submicron device fabrication. The parameters required for KLMC are exactly the information available from *ab-initio* or MD calculations — interaction energies versus distance and transition rates as a function of configuration. KLMC thus provides a natural bridge between fundamental calculations and macroscopic behavior for continuum simulations.

A key application of KLMC has been in understanding donor diffusion at high concentrations. We have found that KLMC simulations of vacancy-mediated dopant diffusion using dopant/vacancy interactions with binding energies from DFT calculations [17, 18] lead to greatly enhanced diffusion for very high doping levels ($> 2 \times 10^{20}$cm^{-3}) [14, 16]. These results are in agreement with the observations of Larsen *et al.* [19] of enhanced diffusion of As, Sb, Sn and Ge in heavily P-doped material (Fig. 5).

These observations are critical to understanding high concentration As diffusion as required for shallow junction technology. A key feature of As profiles is a mismatch between active doping level and the much higher (by order of magnitude) apparent solubility associated with shoulder of diffusion profile [21]. Although DFT calculations indicate that As deactivation is due to immobile As_nV clusters [22, 23], the high concentration diffusion effect illustrated in Fig. 5 can account for this otherwise anomalous behavior (Fig. 6). Because of the dramatic increase of diffusivity at high doping doping levels, the small gradient in free As concentration associated with dominant As_4V clusters leads to a large diffusion flux.

A second key element required for matching shallow junction active and chemical profiles is incorporation of V in regrown region due to high As concentrations [25]. The effect is similar to what we propose for F, but 2 neighboring As atoms are required since As/V binding is weaker than F/V binding. This effect allows rapid As deactivation without too much diffusion due to I injection from As_4 clusters [25]. This picture is supported by positron annihilation experiments [26] which find a large vacancy population in laser annealed samples, and by reduction of {311} defects and loops in high dose low energy As implanted silicon formed [27].

Reduced device dimensions and thermal budgets greatly reduce computation times for KLMC simulations, while requiring the inclusion of complex non-equilibrium behavior that makes continuum simulations more computationally expensive. Thus KLMC simulations become a realistic alternative for simulation of deep submicron structures. 3D KLMC simulations of sub-100nm nMOS

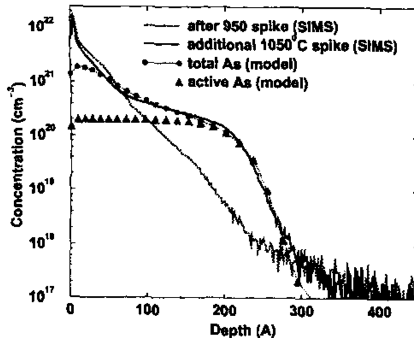

Figure 6: Comparison of simulation and experiment for 2×10^{15} cm^{-2} 5 keV As$^+$ implant for 1050°C spike anneal following 950°C spike. Data from Jain [24].

structures have previously been demonstrated [15]. Such atomistic simulations become necessary for deep submicron devices because the modest number of dopants and defects present lead to significant variations in device properties. To accurately model these effects, it is necessary to include electric field effects on dopant redistribution, which have previously been neglected in atomistic simulations.

To model the potential distribution near charged defects, we use the quantum perturbation method. We find that the resulting distribution matches the classical screened Coulombic potential at large distances, but is very different at short range (<1nm) as it avoids the singularity at the origin [28]. Including the local charge distributions and associated potential variations leads to both standard behavior seen in continuum simulations (e.g., concentration-dependent diffusion, electric field effects at junctions), as well as unique atomistic effects. A key example of the latter is that Coulombic repulsion leads to ordering in the distribution of dopants, reducing potential fluctuations and thus threshold voltage variations in nanoscale devices [28].

IV. CONCLUSIONS

We have illustrated some of the ways in which atomistic calculations can be effectively used to advance VLSI process modeling. There is clearly great potential for such methods to play an increasingly important role in advancing silicon technology.

ACKNOWLEDGEMENTS

This paper describes the efforts of many collaborators, including current and former students Marius Bunea, Srinivasan Chakravarthi, Milan Diebel, Pavel Fastenko and Zudian Qin, and Hannes Jónsson (UW Chemistry) and his research group, particularly Blas Uberuaga and Graeme Henkelman. The work was supported primarily by the SRC.

REFERENCES

[1] X.-Y. Liu, W. Windl and M.P. Masquelier, *Appl. Phys. Lett.* **77**, 2018 (2000).

[2] T.J. Lenosky, B. Sadigh, S.K. Theiss, M.J. Caturla, and T. Diaz de la Rubia, *Appl. Phys. Lett.* **77**, 1834 (2000).

[3] G. Henkelman and H. Jónsson, *J. Chem. Phys.* **111**, 7010 (1999).

[4] H. Jónsson, G. Mills and K.W. Jacobsen, in *Classical and Quantum Dynamics in Condensed Phase Simulations*, ed. B. J. Berne, G. Ciccotti, and D. F. Coker (World Scientific, 1998) p. 385.

[5] B.P. Uberuaga, G. Henkelman, H. Jónsson, S.T. Dunham, W. Windl and R. Stumpf, ICCN 2001 Proc., pp. 101–104; *ibid, Phys. Stat. Sol. B* (2002).

[6] S. Chakravarthi and S.T. Dunham, *J. Appl. Phys.* **89**, 3650 (2001)

[7] P. Fastenko, S.T. Dunham and S. Chakravarthi, *MRS Proc.* **717**, C5.3 (2002).

[8] T.H. Huang and D.L. Kwong, *Appl. Phys. Lett.* **65**, 1829 (1994).

[9] J. Park and H. Hwang, *MRS Proc.* **568**, 71 (1999).

[10] D.F. Downey, J.W. Chow, E. Ishida and K.S. Jones, *Appl. Phys. Lett.* **73**, 1263 (1998).

[11] L.S. Robertson, P.N. Warnes, K.S. Jones, S.K. Earles, M.E. Law, D.F. Downey, S. Falk and J. Liu, *MRS Proc.* **610**, B4.2.1 (2000).

[12] S.-P. Jeng, T.-P. Ma, R. Canteri, M. Anderle and G.W. Rubloff, *Appl. Phys. Lett.* **61**, 1310 (1992).

[13] M. Diebel and S.T. Dunham, *MRS Proc.* **717**, C4.5 (2002).

[14] S.T. Dunham and C.D. Wu, *J. Appl. Phys.* **78**, 2362 (1995).

[15] M.M. Bunea and S.T. Dunham, *MRS Proc.* **490**, 3 (1998).

[16] S.T. Dunham and Z. Qin in *2001 International Conference on Simulation of Semiconductor Process and Devices (SISPAD 2001)*, D. Tsoukalas and C. Tsamis, eds. (Springer-Verlag, Vienna, 2001) pp. 116–119.

[17] O. Pankratov, H.C. Huang, T. Diaz de la Rubia, *et al.*, *Phys. Rev. B***56**, 13172 (1997).

[18] J.S. Nelson, P.A. Schultz and A.F. Wright, *Appl. Phys. Lett.* **73**, 247 (1998).

[19] A.N. Larsen, K.K. Larsen, P.E. Andersen and B.G. Svensson, *J. Appl. Phys.* **73**, 691 (1993).

[20] R.B. Fair and G.R. Weber, *J. Appl. Phys.* **44**, 273 (1973).

[21] D. Nobili, S. Solmi, A. Parisini, M. Derdour, A. Armigliato and L. Moro, *Phys. Rev. B* **49**, 2477 (1994).

[22] M. Berding and A. Sher, *Phys. Rev. B* **58**, 3853 (1998).

[23] J. Xie and S.P. Chen, *J. Appl. Phys.* **87**, 4160 (2000).

[24] A. Jain, SIMS and resistivity data from Texas Instruments.

[25] P. Fastenko, S.T. Dunham and G. Henkelman, *MRS Proc.* **669**, J5.10 (2000).

[26] D.W. Lawther, U. Myler, P.J. Simpson, P.M. Rousseau, P.B. Griffin, W.T. Fang and J.D. Plummer, *Appl. Phys. Lett.* **67**, 3575 (1995).

[27] V. Krishnamoorthy, A. Moller, K.S. Jones, D. Venables, J. Jackson and L. Rubin, *J. Appl. Phys.* **84**, 5997 (1998).

[28] Z. Qin and S.T. Dunham, *MRS Proc.* **717**, C3.8 (2002).